Cancer Letters 445 (2019) 1–10

Contents lists available at ScienceDirect

Cancer Letters

journal homepage: www.elsevier.com/locate/canlet

Original Articles

Synthesis and biological evaluation of *N*-biphenyl-nicotinic based moiety compounds: A new class of antimitotic agents for the treatment of Hodgkin Lymphoma

L. Porcelli[a], D. Stolfa[a,b], A. Stefanachi[b], R. Di Fonte[a], M. Garofoli[a], R.M. Iacobazzi[a], N. Silvestris[c], A. Guarini[d], S. Cellamare[b], A. Azzariti[a,*]

[a] Experimental Pharmacology Laboratory, IRCCS Istituto Tumori Giovanni Paolo II, Bari, Italy
[b] Dipartimento di Farmacia-Scienza del Farmaco, Università di Bari, Bari, Italy
[c] Medical Oncology Unit, IRCCS Istituto Tumori Giovanni Paolo II, Bari, Italy
[d] Haematology Unit, IRCCS Istituto Tumori Giovanni Paolo II, Bari, Italy

ARTICLE INFO

Keywords:
Novel microtubule-targeting agents
N-biphenylanilides
Hodgkin Lymphoma cell lines
Capillary morphogenesis

ABSTRACT

We previously demonstrated that some *N*-biphenylanilides caused cell-cycle arrest at G2/M transition in breast cancer cells. Among them we choose three derivatives, namely PTA34, PTA73 and RS35 for experimentation in solid tumor cell lines, classical Hodgkin Lymphoma (cHL) cell lines and bona fide normal cell lines. Almost all tumor cells were sensitive to compounds in the nanomolar range whereas, they were not cytotoxic to normal ones. Interestingly the compounds caused a strong G2/M phase arrest in cHL cell lines, thus, here we investigated whether they affected the integrity of microtubules in such cells. We found that they induced a long prometaphase arrest, followed by induction of apoptosis which involved mitochondria. PTA73 and RS35 induced the mitotic arrest through the fragmentation of microtubules which prevented the kinethocore-mitotic spindle interaction and the exit from mitosis. PTA34 is instead a tubulin-targeting agent because it inhibited the tubulin polymerization as vinblastine. As such, PTA34 maintained the Cyclin B1-CDK1 regulatory complex activated during the G2/M arrest while inducing the inactivation of Bcl-2 through phosphorylation in Ser70, the degradation of Mcl-1 and a strong activation of BIML and BIMS proapoptotic isoforms. In addition PTA34 exerted an antiangiogenic effect by suppressing microvascular formation.

1. Introduction

The clinical and basic research in cancer treatment frequently faces high cytotoxicity to non-tumorigenic cells and multiple cancer resistance, developed in response to highly validated chemotherapeutics. Among antimitotic drugs, the microtubules targeting agents (MTAs) such as taxanes and vinca alkaloids are used in several hematological malignancies and solid tumors [1]. They are categorized in destabilizers that bind to tubulin and avoid microtubule polymerization such as vinca alkaloids and in stabilizers which in contrast are agents that bind to tubulin and stabilize microtubule polymer, such as taxanes. Both classes of drugs, by suppressing the spindle-microtubule dynamics, block mitosis at the metaphase–anaphase transition and induce apoptotic cell death through the activation of the CDK1/cyclin B complex and the rapid phosphorylation/inactivation of the anti-apoptotic protein Bcl-2, which is regarded as a hallmark of MTAs functionality because of its role as “guardian of microtubule integrity” [2]. However, despite their clinical success, MTAs are highly toxic to normal cells, therefore there is an urgent need for the discovery of new, more effective and less toxic molecules, which once validated become novel therapeutics, principally for refractory or relapsed patients. Some years ago, some of us started a medium screening program of in-house chemical libraries for identification of new antiproliferative substances, selected from a set of newly synthesized P-gp modulators [3]. Most of the substances showed intrinsic cytotoxicity towards MCF7-ADR cell line resistant to doxorubicin [4]. This evidence encouraged us to expand the series including non-trimethoxy anilides members such as some nicotinamide derivatives. In 2017 we published a new series of

Abbreviations: cHL, classical Hodgkin Lymphoma; MTAs, Microtubules Targeting Agents; HMVEC, Human Microvascular Endothelial Cells; TLC, Thin Layer Chromatography; NHDF-Ad, Normal Human Dermal Fibroblasts-Adult; HRS, Hodgkin-Reed Stemberg

* Corresponding author. Experimental Pharmacology Laboratory, IRCCS Istituto Tumori Giovanni Paolo II, Viale O. Flacco, 65, 70124, Bari, Italy.
E-mail address: a.azzariti@oncologico.bari.it (A. Azzariti).

https://doi.org/10.1016/j.canlet.2018.12.013
Received 17 July 2018; Received in revised form 5 December 2018; Accepted 11 December 2018

nitrobiphenyl nicotinamides that displayed a noteworthy anti-proliferative activity against MCF-7 and MDA-MB-231 breast tumor cell lines [5] and interestingly some of them induced a dose-dependent accumulation of G2/M-phase cell population in MCF7 like vinblastine. This prompted us to investigate if they blocked mitosis by suppressing the spindle-microtubule dynamics. Among such compounds we choose PTA34, PTA73 and RS35 and here, in order to report the identification and pharmacologic characterization of such *N*-biphenylanilides as a novel, highly potent and selective class of MTAs we evaluated their effect on tubulin polymerization and their antitumor activity in a panel of tumor cells and normal cells. The focus was the molecular and morphological features of mitotic arrest and apoptosis induction in Hodgkin Lymphoma cell lines. In addition, because some MTAs have recently received considerable interest as potential anti-angiogenic and vascular-disrupting agents, we tested the potential antiangiogenic effect, by assessing the ability to disrupt capillary morphogenesis of human microvascular endothelial cells (HMVEC).

2. Materials & methods

2.1. Reagents and procedures

High analytical grade chemicals and solvents were purchased from commercial suppliers. When necessary, solvents were dried by standard techniques and distilled. After extraction from aqueous layers, the organic solvents were dried over anhydrous sodium sulfate. Thin layer chromatography (TLC) was performed on aluminum sheets precoated with silica gel 60 F254 (0.2 mm) (E. Merck). Chromatographic spots were visualized by UV light. Purification of crude compounds was carried out by flash column chromatography on silica gel 60 (Kieselgel 0.040–0.063 mm, E. Merck) or by preparative TLC on silica gel 60 F254 plates or crystallization. ^{1}H NMR spectra were recorded in DMSO-d_6 or $CDCl_3$ at 300 MHz on a Varian Mercury 300 instrument. Chemical shifts (δ scale) are reported in parts per million (ppm) relative to the central peak of the solvent. Coupling constant (J values) are given in hertz (Hz). Spin multiplicities are given as s (singlet), br s (broad singlet), d (doublet), t (triplet), dd (double doublet), dt (double triplet), or m (multiplet). LRMS (ESI) was performed with an electrospray interface ion trap mass spectrometer (1100 series LC/MSD trap system Agilent, Palo Alto, CA). In all cases, spectroscopic data are in agreement with assigned structures. Combustion analyses were performed by Eurovector Euro EA 3000 analyzer (Milan, Italy) and gave satisfactory results (C, H, N within 0.4% of calculated values). The synthesis of compound PTA34 was already described [5].

2.1.1. Procedure for the Suzuki-Miyaura cross-coupling reaction: preparation of compounds 3-nitro-[1,1′-biphenyl]-4-amine a (Scheme 1)

A suspension of the 4-bromo-2-nitroaniline (1, 04 g, 5.0 mmol), benzene boronic acid (0,92 g, 7.5 mmol), and Pd(PPh3)4 (0.58 g, 0.50 mmol) in a 2 M aqueous solution of K2CO3 (7.5 ml) and 1,4-dioxane (30 mL) was heated at 100 °C for 3 h under stirring. After cooling, the solvent was evaporated under vacuum to dryness and the obtained residue was treated with dichloromethane. The suspension was filtered on celite and the resulting residue was purified by silica gel column chromatography.

Yield: 50%. Eluent: Hexane 8/AcOEt 2.

^{1}HNMR ($CDCl_3$) δ:8.38 (1H, d, J = 2.1 Hz), 7.65 (1H, dd, J = 2.1 Hz, J = 8.7 Hz), 7.58–7.54 (2H, m), 7.44 (2H), 7.38–7.30 (1H, m), 6.90 (1H, d, J = 8.7 Hz), 6.11 (2H, br s). LRMS (ESI) m/z 213.1 [M-H]-.

2.1.1.1. Synthesis of N-(3-nitro-[1,1′-biphenyl]-4-yl)nicotinamide (PTA 73). The intermediate aniline a (0, 21 g, 1 mmol) was dissolved in 10 ml of dry dioxane and then nicotinoyl chloride hydrochloride (0,53 g, 3 mmol), DMAP (0, 12 g, 1 mmol) and triethylamine (2 mmol, 0.278 mL) were added. The mixture was refluxed for 18 h. After cooling the obtained precipitate was removed by filtration. The filtrate was evaporated and the residue was purified by silica gel column chromatography.

Yield: 32%. m.p.: 175–177 °C. Eluent: Hexane 7/AcOEt 3.

^{1}HNMR ($CDCl_3$) δ: 11.40 (1H, s), 9.28 (1H, d, J = 2.1 Hz), 9.05 (1H, d, J = 8.8 Hz), 8.85 (1H, dd, J = 1.6 Hz, J = 4.6 Hz), 8.53 (1H, d, J = 2.1 Hz), 8.30 (1H, dt, J = 1.6 Hz, J = 6.6 Hz), 7.98 (1H, dd, J = 2.1 Hz, J = 8.8 Hz), 7.66–7.60 (2H, m), 7.54–7.47 (3H, m), 7.47–7.39 (1H, m). LRMS (ESI) m/z 318.0 $[M-H]^{-\cdot}$

2.1.1.2. Synthesis of N-(3-nitro-[1,1′-biphenyl]-4-yl)pyrimidine-5-carboxamide (RS 35). The starting pirimydin carboxilic acid (1.5 mmol) was suspended under argon in thionyl chloride (2.0 mL) and stirred for 3 h at room temperature. The unreacted excess of thionyl chloride was removed under nitrogen flow to afford the corresponding benzoyl chloride. The solid thus obtained was used without further purification in the condition described above to react with aniline. Yield: 10%. m.p. 218–220 °C:. Eluent: Hexane 8/AcOEt 2.

1HNMR (CDCl3) δ: 11.44 (1H, br s), 9.45 (1H, s), 9.35 (2H, s), 9.02 (1H, d, J = 8.8 Hz), 8.54 (1H, d, J = 2.1 Hz), 8.0 (1H, dd, J = 2.1 Hz, J = 8.8 Hz), 7.65–7.62 (2H, m), 7.54–7.43 (3H, m).

LRMS (ESI) m/z 319.0 $[M-H]^-$

2.2. In vitro tubulin polymerization assay

PTA34, PTA73 and RS35 were tested at 3 μm concentration in a tubulin polymerization assay, by using the kit (Cytoskeleton Inc., Denver, CO, USA) (Tubulin polymerization assay, Cytoskeleton, Inc.: http://www.cytoskeleton.com/bk011p). Lyophilized tubulin (Cytoskeleton) was used to evaluate the tubulin polymerization inhibiting activity. Vinblastine and paclitaxel at 3.0 μm were used as positive controls for tubulin polymerization inhibition and stabilization, respectively. All compounds were dissolved in DMSO and further diluted with sterile water to obtain a maximum DMSO concentration of 0.1%, which was used as solvent control. Polymerization was monitored by fluorescence enhancement due to the incorporation of a

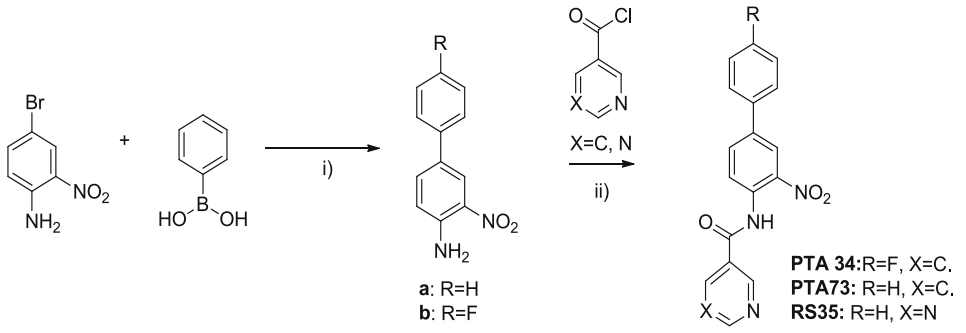

Scheme 1. Reaction of synthesis of PTA34, PTA73 and RS35.

fluorescent reporter into microtubules as polymerization occurred. In a 96 well plate, to a 0.5 mL of a 100 V stock solution of each compound, 49.5 mL of supplemented tubulin supernatant were added. Incubation was done in a temperature-controlled Multi-label Microplate Fluorimeter, equipped with filters for excitation at 340–360 nm and emission at 420–460 nm (Victor 3 Model 1420-01296, PerkinElmer, Inc. MA, USA) at 378C, and fluorescence was measured at 460 nm every minute for 60 min according to the recommended procedures.

2.3. Drugs and chemicals

PTA34, PTA73 and RS35 were dissolved in DMSO. Further dilutions were made in medium supplemented with 10% foetal bovine serum, 2 mM glutamine, 50,000 UL-1 penicillin and 80 μM streptomycin.

2.4. Cell lines

The classical Hodgkin lymphoma cell lines KM-H2, HDLM-2, L540, L428 and L1236 [6] were generously provided by Prof. Rosaria De Filippi (University of Naples Federico II, Italy) and authenticated through STR profile at the beginning of experiments. They were routinely cultured in IMDM (Iscove's modified Dulbecco's MEM) supplemented with 10% fetal bovine serum, 100 U/ml penicillin, 100 μg/ml streptomycin. The panel of solid tumor cells encompasses breast cancer cell lines MCF7, HCC1937 and MDA-MB-468; colon cancer cell lines Colo205, LoVo and KM-12; pancreatic cancer cell lines Panc-1, AsPC-1 and MIA PaCa-2 and ovarian cancer cell lines SK-OV-3 and Caov-3. All cells were purchased from ATCC. Breast cancer cells MCF7 were cultured in Eagle's Minimum Essential Medium (EMEM) supplemented with 0.01 mg/ml human recombinant insulin and with 10% fetal bovine serum; MDA-MB468 cells were cultured in Leibovitz's L15 medium supplemented with 10% fetal bovine serum and HCC1937 were cultured in RPMI-1640 medium supplemented with fetal bovine serum to a final concentration of 10%. Colon cancer cells Colo205 were cultured in RPMI-1640 medium with 10% fetal bovine serum; LoVo were cultured with F-12 K with 10% fetal bovine serum and Km 12 were cultured in RPMI-1640 medium supplemented with fetal bovine serum to a final concentration of 10%Pancreatic cancer cells Panc-1 were culture in Dulbecco's Modified Eagle's medium supplemented with fetal bovine serum to a final concentration of 10%; AsPC-1 were cultured in RPMI-1640 medium with fetal bovine serum to a final concentration of 10% and MIAPaCa-2 were cultured in Dulbecco's Modified Eagle's Medium with the addition of fetal bovine serum to a final concentration of 10% and horse serum to a final concentration of 2.5%. Ovarian cancer cells Caov-3 were cultured with Dulbecco's Modified Eagle's Medium, supplemented with fetal bovine serum to a final concentration of 10% and SK-OV-3 with McCoy's 5a medium with fetal bovine serum to a final concentration of 10%. Human Dermal Microvascular Endothelial Cells (HMVEC) were purchased from Lonza and cultured in EGM-2 Endothelial Growth Medium, EGM™-2 MV BulletKit™ from Lonza. NHDF-Ad Human Dermal Fibroblasts, Adult were purchased from Lonza and cultured in FGM2 (Fibroblast Growth Medium-2 BulletKit™ from Lonza). cHL cell lines, solid tumor cell lines HMVEC and NHDF-Ad were cultured in a humidified incubator at 37 °C with an atmosphere containing 5% CO2. MDA-MB-468 were cultured in a free gas exchange incubator at 37 °C with atmospheric air.

2.5. Cell proliferation assay

Determination of cell growth inhibition was performed using the Cell Counting Kit-8 (Sigma-Aldrich), after exposing cells to increasing concentrations of compounds for 24 and 72 h in HRS cells and the MTT assay for adherent cells. The IC_{50} was defined as the drug concentration yielding a fraction of affected (no surviving) cells = 0.5, compared with untreated controls and was calculated utilizing CalcuSyn ver.1.1.4 software (Biosoft, UK).

2.6. Cell cycle analysis

After two wash steps in ice-cold PBS (pH 7.4), cells were fixed in 4.5 ml of 70% ethanol and stored at −20 °C. For the analysis, the pellet was resuspended in PBS containing 1 mg/ml RNase, 0.01% NP40 and 50 μg/ml propidium iodide (PI) (Sigma). After an incubation time of 1 h in ice, cell cycle determinations were performed using a FACScan flow cytometer (Becton Dickinson), and data were interpreted using the CellQuest software, provided by the manufacturer.

2.7. Immunofluorescence on cells in suspension

Cell suspension was transferred to microcentrifuge for spinning. After two wash step in PBS 1X, cells were spiked in 3.7% PFA and incubated at room temperature for 15 min. After two wash steps in PBS 1X, cells were permeabilized with 0.3% Triton X-100 in PBS 1X for 5 min. Non-specific binding sites were blocked for 30 min at room temperature with PBS containing 5% BSA and then cells were incubated with a mouse anti-α-tubulin monoclonal antibody (Sigma-aldrich) diluted in PBS containing 4% BSA for 60 min at room temperature. The staining of α-tubulin was followed by incubation with FITC-conjugated anti-mouse antibody. After two wash steps in PBS 1X, the remaining liquid was carefully aspirated and the cells pellet was resuspended in Vectashield with Dapi (Vector Laboratories), dropped on slides and covered with coverslip for microscope examination (Leica).

2.8. Cell apoptosis assays

Apoptosis detection was investigated by the Cell Death ELISAPLUS kit (Roche Molecular Biochemicals, Milan, Italy) and the AnnexinV/PI assay (Becton Dickinson) followed by flow cytometry (FACScan). The first is based on the detection of mono- and oligonucleosomes in the cytoplasmic fraction of cell lysates by biotinylated anti histone-coupled antibodies, and their enrichment in the cytoplasm is calculated as the absorbance of sample cells/absorbance of control cells. The enrichment factor was used as a parameter of apoptosis and shown on the Y-axis as mean ± SE. Experiments were performed according to manufacturer's instructions. The second is a double-staining method based on the analysis of phosphatidylserine exposure on the cell membrane by an Annexin-V FITC/propidium iodide staining and allows detection of early apoptosis as Annexin V positive cells and late apoptosis as Annexin V/PI positive cells.

2.9. Western blot analysis

Protein extracts were obtained by homogenization in RIPA buffer (0.5 M NaCl, 1% Triton X100, 0.5% NP40, 1% deoxycolic acid, 3.5 mM SDS, 8.3 mM Tris HCl pH 7.4, 1.6 mM Tris base) added with protease inhibitor cocktail (Sigma-Aldrich). Total proteins were measured and analyzed as described in Ref. [7]. Briefly 50 μg of total lysates were electrophoretically separated on 10% acrylamide gel (SDS–PAGE by Laemli). Signal was detected by chemoluminescence assay (ECL-Plus, Amersham Life Science, UK). All monoclonal antibodies utilized were provided by Cell Signalling-USA and Sigma-Aldrich, St. Louis, MO-USA. A mouse-HRP and a rabbit-HRP (Amersham Pharmacia Biotech, Upsala Sweden) were used as secondary antibody. β-actin expression was utilized as loading control.

2.10. Detection of mitochondrial transmembrane potential using flow cytometry

Changes in mitochondrial membrane potential were detected by using 5,5′,6,6′-tetrachloro-1,1′,3,3′ tetraethyl benzimidazolylcarbocyanine iodide/chloride (JC-1), a cationic dye that exhibits potential-dependent accumulation in mitochondria. Mitochondrial membrane depolarization was indicated by a reduction of red fluorescence emission

(JC-1 dimers monitored in FL2) and by an increase of green fluorescence emission (JC-1 monomers monitored in FL1) with flow cytometry. Untreated and treated cells were collected, washed with phosphate buffered saline (PBS), stained and analyzed through a flow cytometer.

2.11. In vitro capillary morphogenesis assay

Matrigel (0.5 ml) was pipetted into 96 well plate for tissue culture and left to polymerize as described in Ref. [8]. Subsequently HMVEC were plated in complete MCDB medium, supplemented with 30% FCS, and 20 mg/ml ECGS. Capillary morphogenesis was also performed in the presence of 1 μM PTA34. The effects on the growth and morphogenesis of endothelial cells were recorded after 3 and 6 h with an inverted microscope (Leica DMi8) equipped with CCD optics and a digital analysis system.

2.12. Statistical analysis

All in vitro experiments were performed in triplicate, and results have been expressed as the mean ± standard deviation (SD), unless otherwise indicated. Statistical differences of in vitro data were assessed by the Student-Newman–Keuls test, while the Two tailed method was utilized for data analysis of Tubulin polymerization assay. P-values lower than 0.05 were considered significant. Statistical analyses were performed using the GraphPad Prism software package version 5.0 (GraphPad Software Inc., San Diego, CA, USA).

3. Results

3.1. Cytotoxicity

The anti-proliferative activity of these novel *N*-biphenylanilides was tested on three breast cancer cell lines, three colon cancer cell lines, three pancreatic cancer cell lines, two ovarian cancer cell lines, five bona fide classical Hodgkin lymphoma cell lines and two bona fide normal cell lines. The cytotoxicity of PTA34, PTA73 and RS35 was evaluated after one and three days of continuous exposure by Cell Counting Kit-8 (CCK-8) proliferation assay in cHL cell lines and by MTT assay in solid tumors and normal cells. All three compounds displayed strong antitumor efficacy in all tumor cell lines, whereas PTA34 and PTA73 did not affect the proliferation of HMVEC and NHDF, thus showing to be safe to the tested normal cells. RS35 slightly reduced cell proliferation (10% of untreated cells) of both normal cell types (data not showed). The 24 h exposure reduced the growth of tumor cells of about 50% at 1 μM in almost all cHL lines (data not shown); hence that concentration was utilized in the following one day time experiments in cHL cell lines; while it was higher in solid tumors (data not shown). Three days continuous exposure lowered the IC_{50}s in the nanomolar range in almost all cells, however collectively the antitumor activity of *N*-biphenylanilides was stronger in cHL cell lines then in solid tumors cells. The IC_{50}s, calculated after three days for all tumor cell lines, are reported in Table 1.

3.2. Tested compounds induced G2/M cell cycle arrest

To verify whether the inhibition of cell proliferation was through the affection of cell cycle progression, we detected the DNA content of cell nuclei by flow cytometry after staining with propidium iodide. For this purpose we treated the cells with each compound at three concentrations (0.01 μM, 0.1 μM and 1 μM) for 18 h, 24 h and 72 h. All compounds induced a G2/M cell-cycle arrest starting from 18 h of exposure in all HL cell lines that further increased after 24 h and interestingly the extent of the arrest at each concentration of drug was stable until 72 h, showing that no mitotic slippage of cells occurred during the time of the arrest (data not showed). PTA34 induced the strongest G2/M arrest from 50% to 70% of cells at 0.1 μM and 1 μM PTA34, respectively, in almost all cell lines compared to the 50% and 60% induced by 1 μM PTA73 and RS35, respectively. PTA73 induced the highest sub-G0/G1 accumulation, namely 20% versus 8% and 11% induced by PTA34 and RS35, respectively. A representative analysis of cell cycle of L1236 is reported in Fig. 1A, whereas the cell cycle phases quantification from three different experiments performed in L1236 is reported in Fig. 1B. Interestingly the strongest arrest at G2/M phase was found only in HRS cells and not in the other tumor cells. In Fig. 1C a representative analysis of cell cycle profile in some solid tumor cell lines, chosen among the most sensitive to compounds, is reported. It shows that following treatment they did not go into mitotic arrest comparable to that of HRS cells. Therefore we decided to investigate the *N*-biphenylanilides as MTAs only in HL cell lines.

3.3. Tested compounds induce morphological features of prometaphase arrest in HRS cells

The morphological features of the nuclei of HRS cell lines were analyzed by fluorescent microscopy after 48 h of treatment with PTA34, PTA73, RS35 at 1 μM after staining with DAPI (Fig. 2). The nuclei of treated cells displayed distinct signs of arrest in the prometaphase stage of mitosis; namely the nuclear membrane disappeared and the chromatin appeared condensed, spread and no chromosomal alignment was detectable, as it happens during metaphase. These morphological features of nuclei suggest that all compounds are mitotic inhibitors of HRS cells.

3.4. Tested compounds cause the disruption of cellular microtubule network in HR cells

Because tested compounds markedly blocked the cell cycle in the M phase, we tested whether they could directly affect the organization of the microtubule network. The microtubule network was visualized by indirect immunofluorescence after staining with α-tubulin, whereas the nuclei were revealed with DAPI staining. In control cells the microtubule network exhibited the normal arrangement with microtubules traversing intricately throughout the cell while the nuclei were compact and round shaped (Fig. 3). In the *N*-biphenylanilides treated cells (1 μM PTA34, PTA73 and RS35) the microtubules were destroyed, while the DAPI staining evidenced that the chromatin appeared condensed; however it was spread and no sign of chromosomal alignment was found, and the most of the cells showed pyknotic and fragmented nuclei indicating apoptotic cells (Fig. 3).

3.5. In vitro tubulin polymerization assay

In order to evaluate whether such compounds interfere with microtubules dynamics, we performed a cell-free tubulin polymerization assay. The progression of tubulin polymerization was examined by monitoring the increase in fluorescence emission at 420 nm (excitation wavelength is 360 nm) for 1 h at 37 °C. Vinblastine and paclitaxel, two known microtubule-targeting agents acting as disassembly and assembly promoters, respectively, were used as controls [9]. The effects on tubulin polymerization of the three substances are shown in Fig. 4. As expected, paclitaxel was a stabilizer of tubulin polymerization at 3 μM concentration, whereas vinblastine at the same concentration acted as an effective inhibitor of tubulin polymerization. 3 μM PTA34 showed to perform an effective inhibition of tubulin polymerization, since it achieved the same endpoint inhibition compared to vinblastine ($p < 0.0001$ PTA34 *vs* control). RS35 was less effective than PTA34 in inhibiting tubulin polymerization whereas PTA73 did not show any appreciable effect on the progression of tubulin polymerization (profile similar to control).

Table 1
Inhibitory effect of *N*-biphenylanilides against human cancer cells.

IC_{50} (μM ± SD)			
Cell Line	PTA34	PTA73	RS35
L540	$59 \times 10^{-3} \pm 0.002$	$548.6 \times 10^{-3} \pm 0.004$	$5.0 \times 10^{-3} \pm 0.0004$
L1236	$1.8 \times 10^{-3} \pm 0.0004$	$0.3 \times 10^{-3} \pm 0.00002$	$3.8 \times 10^{-3} \pm 0.005$
L428	$30.4 \times 10^{-3} \pm 0.002$	$2.3 \times 10^{-3} \pm 0.0004$	$1.0 \times 10^{-3} \pm 0.0003$
HDLM-2	$268.4 \times 10^{-3} \pm 0.004$	$13.4 \times 10^{-3} \pm 0.0006$	$1.1 \times 10^{-3} \pm 0.0005$
KM-H2	$63.9 \times 10^{-3} \pm 0.002$	$0.2 \times 10^{-3} \pm 0.00006$	$0.2 \times 10^{-3} \pm 0.0001$
Colo205	1.15 ± 0.5	0.24 ± 0.12	0.1 ± 0.04
LoVo	0.63 ± 0.2	0.1 ± 0.02	0.17 ± 0.02
Km 12	0.88 ± 0.5	0.74 ± 0.6	0.19 ± 0.05
MCF-7	1.5 ± 0.9	2.611 ± 0.4	5.34 ± 1.1
MDA-MB-468	0.88 ± 0.05	0.26 ± 0.05	5.47 ± 0.8
HCC1937	6 ± 0.1	3.6 ± 0.5	6.3 ± 0.6
Panc-1	1.9 ± 0.2	0.9 ± 0.3	1.02 ± 0.05
AsPC-1	1.8 ± 0.3	1.6 ± 0.2	1.5 ± 0.1
MIA PaCa-2	0.3 ± 0.1	0.006 ± 0.001	1.7 ± 0.3
SK-OV-3	21.1 ± 1.2	2.6 ± 0.2	33.2 ± 1.1
Caov-3	0.15 ± 0.05	0.06 ± 0.004	0.07 ± 0.01

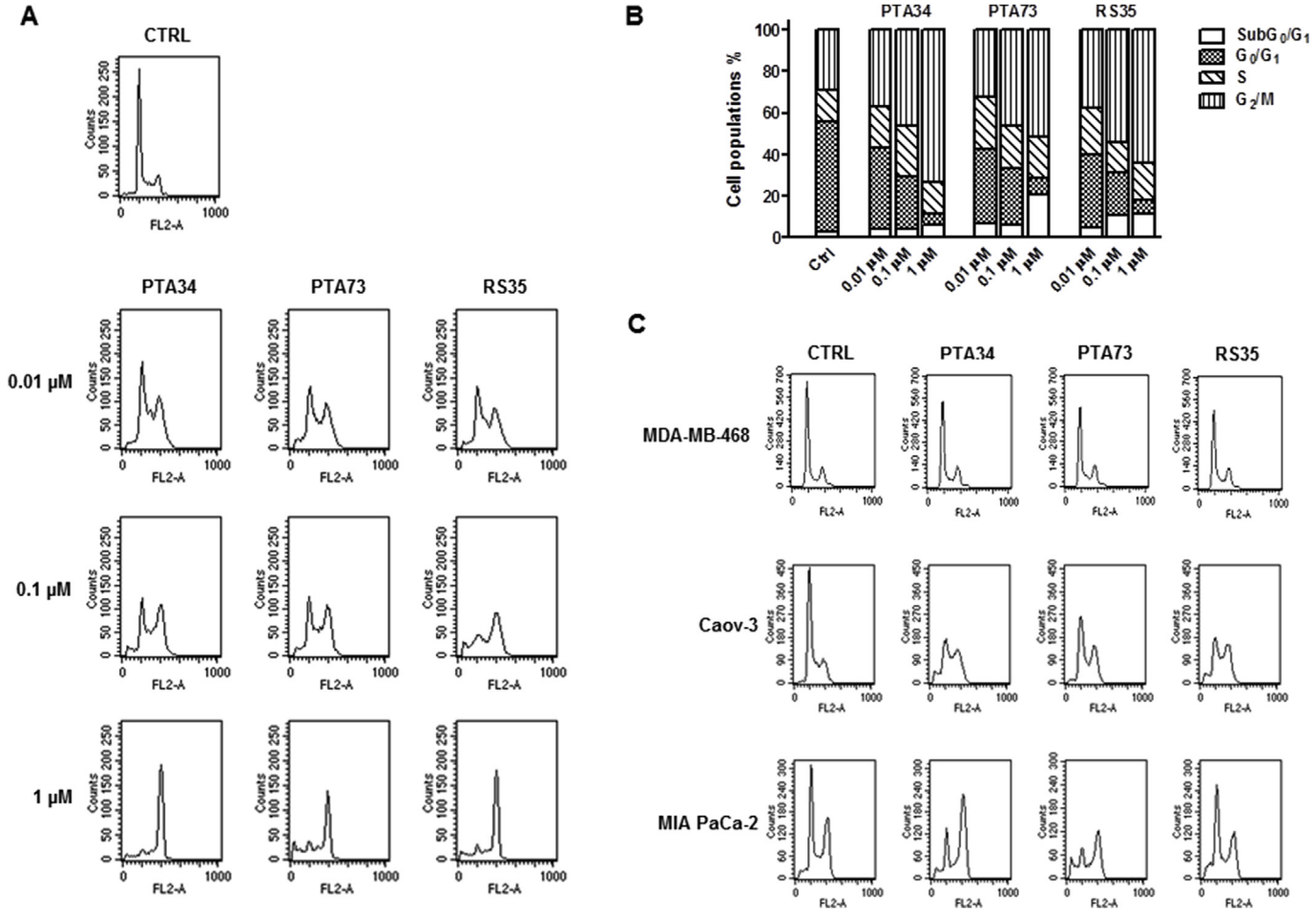

Fig. 1. Effects on cell cycle of L1236 by 0.01–0.1-1 μM PTA34, PTA73 and RS35. The modulation of cell cycle phases was evaluated by FACS after staining cells with propidium iodide. In panel A, a representative analysis of three independent experiments is reported. In panel B the bar graph shows cell population % in each phase of cell cycle, demonstrating that all compounds induced a concentration dependent increase of G2/M phase cell population. In panel C a representative analysis of cell cycle profile shows that, following treatment with 1 μM of all compounds, MDA-MB468, Caov-3 and MIA PaCa-2 did not go into mitotic arrest comparable to that of HRS cells.

3.6. Tested compounds induced apoptosis by causing mitochondrial ΔΨ loss

To assess whether the mitotic arrest, was followed by induction of apoptosis we utilized the FITC Annexin V staining to identify apoptosis at an earlier stage (24 h) and a cell death Elisa assay after 72 h of treatment to measure DNA fragmentation and histone release from the nucleus, occurring during late stage of apoptosis. To carry on both apoptosis assays we treated cells with PTA34, PTA73 and RS35 at

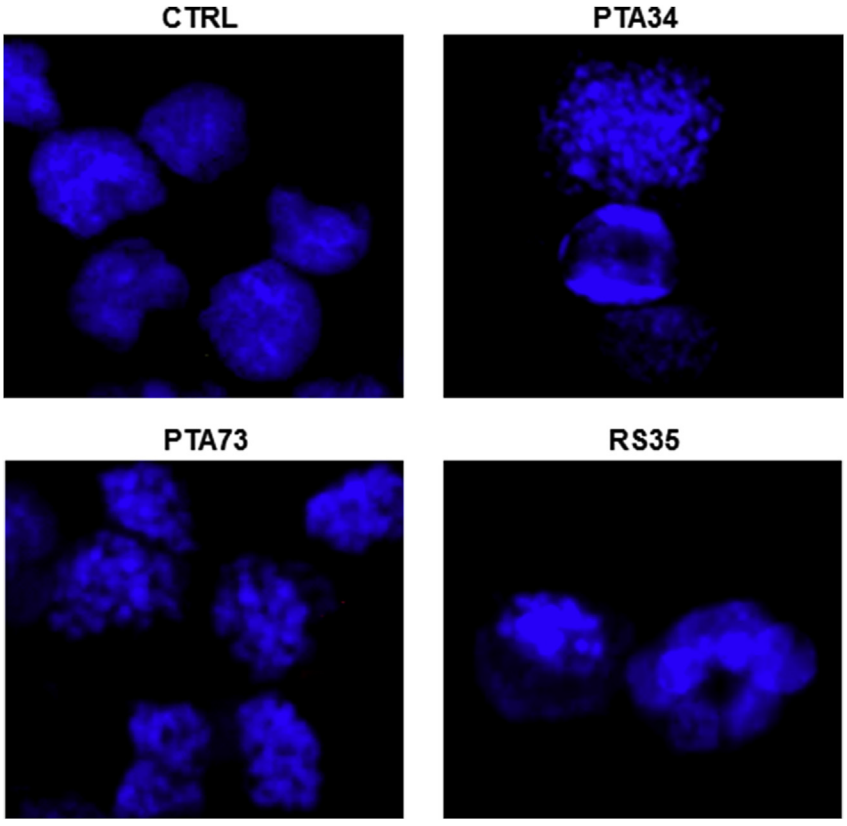

Fig. 2. Immunofluorescent detection of nuclei in L540 cells after 1 μM PTA34, PTA73 and RS35. Nuclei were stained with dapi and the specimens were examined using a Leica (DMi8) immunofluorescence microscope. Reported are images recorded with 100X magnification. The staining evidenced changes of nuclei morphology indicating inhibition of promethaphase-methapahase transition in treated cells compared to untreated ones.

0.1 μM and 1 μM. We found that whilst all compounds induced in L540 a time and concentration dependent (not showed) induction of early apoptosis starting from 24 h and of a significant late apoptosis starting from 72 h of treatment; in other cells such as KMH2 and L1236 cells, the onset of late apoptosis occurred already after 24 h of treatment and increased with the concentration and time exposure. A representative analysis of Annexin V/PI apoptosis performed by FACS in L540 cells is reported In Fig. 5A, whereas the fold change of Annexin V (early apoptosis) and AnnexinV/PI (late apoptosis) positive cells in treated samples versus untreated ones is reported in Fig. 5B. The results are representative of three distinct experiments performed in such cells. Fig. 5C reports a time and concentration dependent evaluation of late apoptosis induced by compounds showing that late apoptosis was already induced at 0.1 μM by all compound in L540.

In order to assess the involvement of mitochondria in the apoptosis, we evaluated the change of mitochondrial membrane potential (depolarization) after treatment with tested compounds. Mitochondrial membrane depolarization was assayed by exposing the cells to JC-1 and visualized as a reduction in the fluorescence signal in the FL2 channel (JC-1 dimers) and increase in FL1 channel (JC-1 monomers). It was assessed after 24 h of treatment with increasing concentration of compounds up to 1 μM in almost all HRS cells. Fig. 6A reports a representative analysis of JC-1 performed by FACS, whereas the quantification of membrane depolarization (JC-1 monomers increase) from experiments performed in L1236, HDLM2 and L540 cells at 1 μM PTA34, PTA73 and RS35 is reported in Fig. 6B. The results are representative of three distinct experiments performed in such cells.

3.7. PTA34 affects cyclin B1 expression and CDK1 activity

The Cdc2 (CDK1)/Cyclin B1 regulatory complex drives progression through G2 and the entrance into and exit out of the M-phase of cell cycle; thus we determined the effects of compounds on CDK1. To this purpose we evaluated the post-translational modifications of CDK1 crucial for its activation and the expression level of Cyclin B1, which is the allosteric activator of CDK1, by evaluating the time course of Cyclin B1 accumulation and destruction and CDK1 phosphorylation at Tyr-15 and Tyr-161 on L540 cell lysates on time 0 and after treatment with PTA34 (1 μM), at 3 h, 6 h, 18 h and 24 h. Fig. 7 reports the immunoblotting of CDK1, demonstrating that while the total CDK1 levels

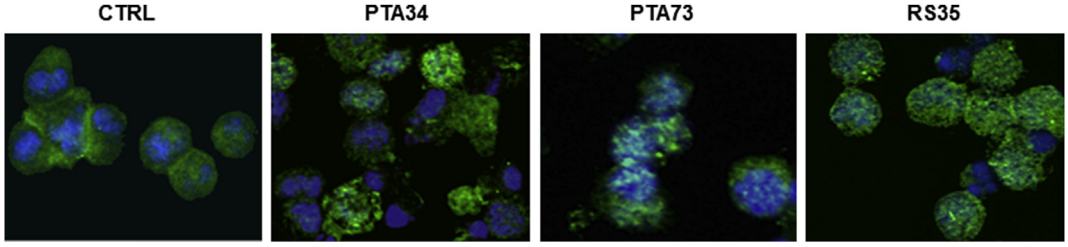

Fig. 3. Immunofluorescent detection of microtubules and nuclei in L540 cells after 1 μM PTA34, PTA73 and RS35. Microtubules were revealed using the primary anti-α-tubulin followed by a FITC-conjugated second antibody. Counterstain of nuclei was with dapi. The specimens were examined using a Leica (DMi8) immunofluorescence microscope. Reported are images recorded with 40X magnification, demonstrating the disruption of microtubules and the formation of pyknotic and fragmented nuclei.

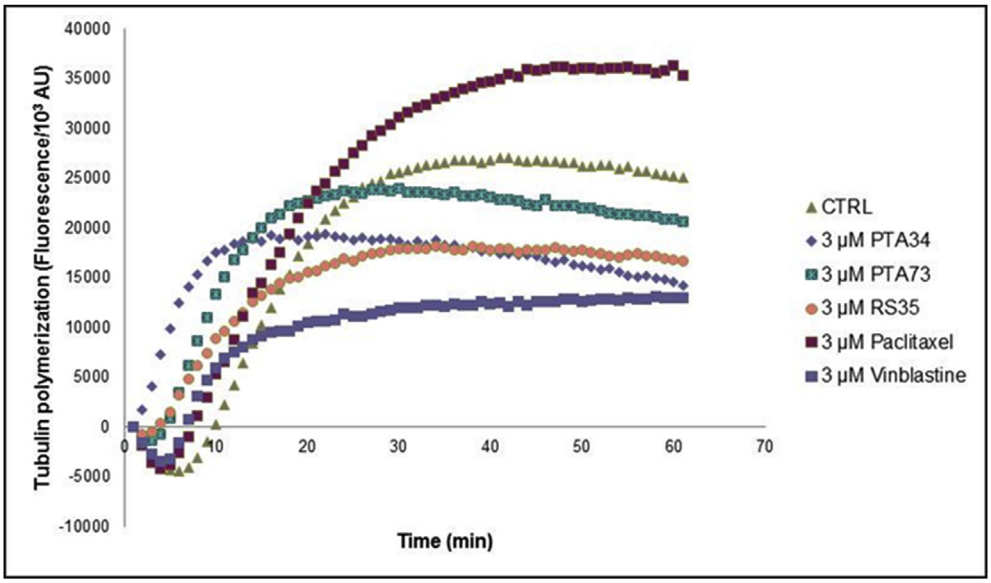

Fig. 4. Effect of PTA34, PTA73 and RS35 on tubulin polymerization. Tubulin polymerization was monitored by the increase of fluorescence at 360 nm (excitation) and 420 nm (emission) for 1 h at 37 °C. All compounds were tested at 3 μM. Paclitaxel and vinblastine were used as positive controls for tubulin polymerization inhibition and stabilization, respectively. The analysis evidenced that PTA34 inhibited tubulin polymerization like vinblastine.

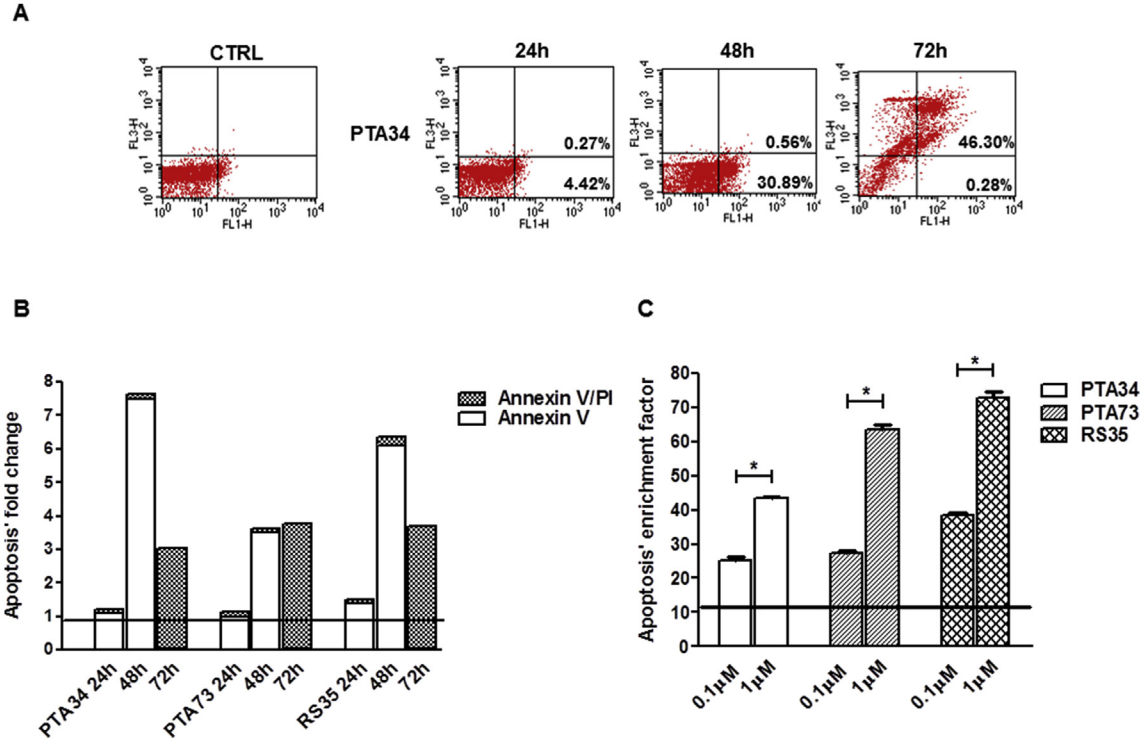

Fig. 5. Induction of apoptosis by PTA34, PTA73 and RS 35. Apoptosis was evaluated, by using Annexin V/PI staining followed by FACS analysis and cell Death Elisa Kit. In Fig. 5A a representative analysis of Annexin V/PI apoptosis performed by FACS is reported, whereas in Fig. 5B the fold change of Annexin V (early apoptosis) and AnnexinV/PI (late apoptosis) positive cells in treated samples versus untreated ones is reported. In Fig. 5C a time and concentration dependent evaluation of late apoptosis induced by compounds is reported showing that late apoptosis was already induced at 0.1 μM by all compound in L540. The results are the mean ± SD of three independent experiments (*p < 0.05).

remained relatively constant along the time course of CDK1 expression evaluation, the levels of CDK1 phosphorylated at Tyr-15 declined from 18 h of treatment with PTA34 until 48 h, while the *p*-CDK1(Y161) was almost stable during the time course of treatment with PTA34, basically indicating that CDK1 was activated during the mitotic arrest elicited by PTA34. Accordingly the level of Cyclin B1 was up regulated starting from 6 h of treatment until 24 h, consistent with a sustained activation of CDK1 along the G2/M blockage of cell cycle. The immunoblots representative of experiments performed in L540 cells are reported in Fig. 7.

3.8. Apoptogenic effect of PTA34 resulted in S70 phosphorylation of Bcl-2, Mcl-1 and Bcl-2 downregulation and activating phosphorylation of pro-apoptotic protein BIM

Because of the pivotal role of Bcl-2 family of proteins in apoptosis, we evaluated the effects of PTA34 on the expression and activation of BH3-only pro-apoptotic protein BIM and on the expression of Bcl-2 and Mcl-1, both playing a key role in the sensitivity to anti-tubulin chemotherapeutics. Furthermore we evaluated the S70 phosphorylation of Bcl-2 which is induced by drugs affecting the integrity of microtubules

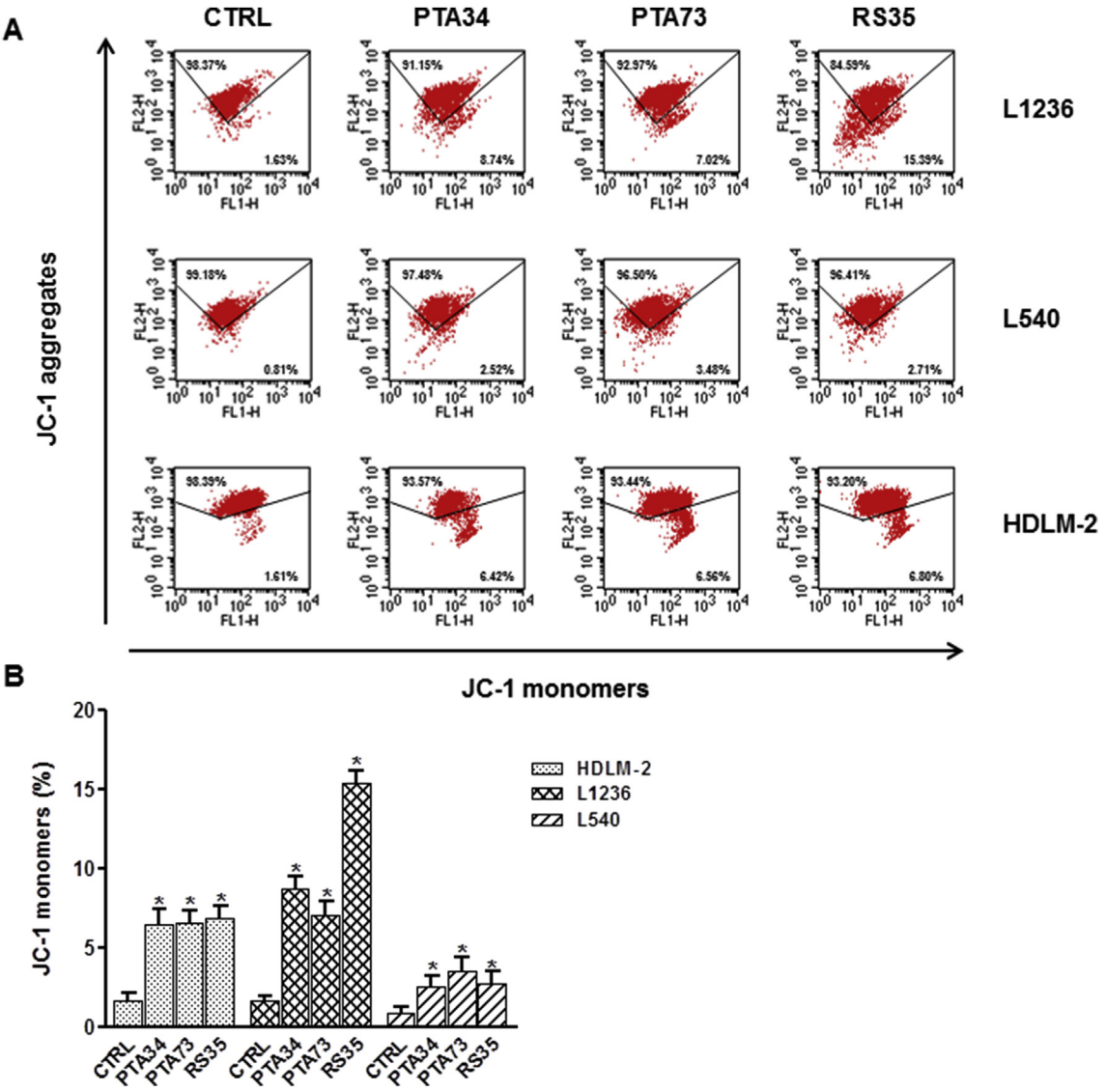

Fig. 6. Effects of compounds on mitochondrial membrane depolarization by JC-1 analysis. Membrane depolarization was visualized as a reduction in the fluorescence signal in the FL2 channel (JC-1 dimers) and as an increase in FL1 channel (JC-1 monomers). In Fig. 6A is reported a representative analysis of JC-1 performed by FACS in HDML-2, L540 and L1236. In Fig. 6B the bar graph shows the percentage of JC-1 monomer-positive cells. The results are the mean ± standard deviation of three independent experiments. *P < 0.05 versus the control.

and is regarded as a post-translational modification which inactivates Bcl-2 anti-apoptotic function [2,10,11]. As shown in Fig. 7, the time course of proteins expression performed on L540 cells treated with PTA34 1 μM, evidenced that Bcl-2 was reduced at 18 h and 24 h, while Mcl-1 started to be down-regulated soon after 3 h of treatment and remained reduced until 24 h. In agreement with the potent induction of apoptosis and with the reduction of Mcl-1, we found a time dependent increase of BIMEL expression starting from 3 h until 48 h of treatment, while BIML and BIMS, which are regarded as the two most apoptotic BIM isoforms [12], started to increase after 18 h and remained strongly expressed until 48 h according with the occurrence of damage to microtubules and apoptosis induction in such cells.

3.9. PTA34 exerts anti-angiogenic effects in vitro

The matrigel in vitro assay was used to evaluate the anti-angiogenic properties of PTA34 on HMVEC cells morphology. The cells were seeded on matrigel in presence of 1 μM PTA34, then the vascular structures formation was evaluated. Interestingly 1 μM of compound, which resulted in no anti-proliferative effect on HMVEC cells after 24 h, exerted a time dependent suppression of microvascular formation starting from 4 h (data not showed) compared to control and resulted in a complete inhibition after 6 h (Fig. 8).

4. Discussion

Targeting of microtubule assembly/disassembly with microtubule inhibitors represents an important therapeutic strategy in both hematopoietic and solid tumors; though the effectiveness of such agents is frequently limited from the onset of resistance and toxicity to normal cells [13]. The nitro-biphenylanilides PTA34, PTA73 and RS35, that in the present work were tested against a panel of cell lines from different solid tumor of origin and Hodgkin lymphoma cell lines, strongly inhibited cell proliferation of almost all cells in the nanomolar range but they selectively caused cell-cycle arrest at G2/M transition of HL cell lines, like the reference compounds vinblastine and paclitaxel. Therefore we started with investigating whether the tested compounds selectively targeted the microtubule system and the underlying mechanisms of antitumor effectiveness, basically in Hodgkin- Reed-Stemberg cells. The results reported herein suggest that all compounds induced a

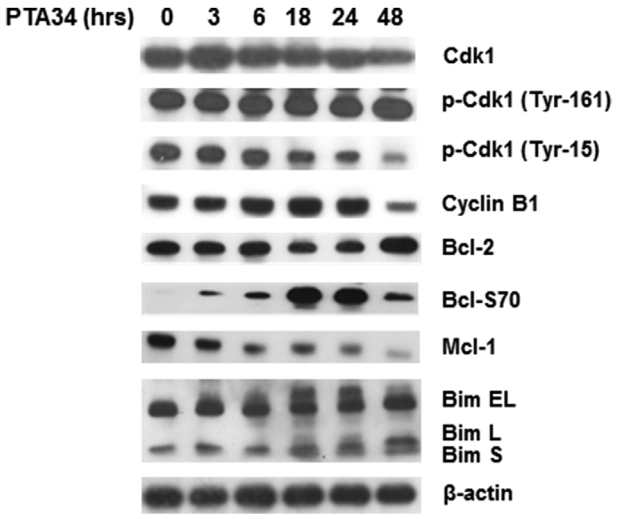

Fig. 7. Time-course of PTA34 effect on protein levels related to mitotic arrest and apoptosis in L540 cells. Protein expression was determined by Western blot analysis using a primary antibody followed by a second HRP-conjugated antibody. For loading differences evaluation, the blots were stripped and reacted with an antibody against β-actin.

promethaphase arrest of HRS cells, however only PTA34 stops the tubulin polymerization comparable to vinblastine, and notwithstanding that, while both PTA73 and RS35, did not affect tubulin polymerization, they resulted in defective mitosis with similar features to PTA34 treated cells. Indeed the immunofluorescence showed that the nuclear envelop was disassembled, the chromatin appeared condensed while no chromosomal alignment was detectable and the microtubules appeared fragmented in compounds treated cells. Thus, perhaps PTA73 and RS35 may have targeted mitotic machinery other than tubulin, as the key players in the kinethocore-mitotic spindle interaction and this has caused a severe misalignment of the chromosomes that affected microtubules spindle dynamics and prevented moving the poles and exiting mitosis. According to the molecular effects elicited by microtubule-targeting drugs, such as paclitaxel and vinblastine, PTA34 was found to induce many of the hallmarks associated with the activity of antimicrotubule agents [14–16]. During mitotis the Cyclin B-Cdc2 kinase is activated to induce entry into M-phase and when all chromosome's kinetochores are attached to microtubules, the anaphase-promoting complex/cyclosome (APC/C) inactivates Cyclin B1-CDK1 by promoting its degradation to reform the nuclear envelope and for exiting the M-phase [17–19]. Accordingly, in PTA34-treated cells the Cyclin B1-CDK1 is kept in an active state during the G2/M arrest and this evidently prevents APC activation and the onset of anaphase. Characteristically during the G2/M phase arrest the microtubules inhibitors induce apoptosis through the inactivation of prominent members of Bcl-2 family of proteins which promote cell survival by blocking/sequestering cell death mediators such as BAX, BAK and BIM [10]. BIM is a potent inducer of apoptosis. In the inactive form, BIM is bound to microtubules through the dynein light chain, while in the presence of microtubule damage, just like after treatment with MTAs, it is released from microtubules to accumulate in mitochondria to trigger apoptosis [20]. PTA34 was found to reduce the expression of the anti-apoptotic proteins Bcl-2 and Mcl-1, both notoriously involved in the sensitivity to MTAs, while it induced a strong increase of the most pro-apoptotic isoforms of BIM, namely BIML and BIMS and consequent mitochondria membrane depolarization. Even more interesting is the sudden and lengthy period of phosphorylation of Bcl-2 induced by PTA34, followed by Bcl-2 dephosphorylation closely correlated with initiation of apoptosis. The latter event is regarded as a switch for induction of apoptosis by vinblastine [21]. Therefore after damaging the microtubules of HRS cells, PTA34 determined the transition from the mitotic block to the induction of apoptosis by eliciting a precise cycle of phosphorylation/dephosphorylation of Bcl-2, the degradation of Mcl-1 and Bcl-2 and the activation of BIM that connected microtubule damage to the induction of apoptosis mediated by mitochondria. Speculating on the activity of mitosis-selective inhibitors, we suggest that *N*-biphenylanilides caused a prolonged arrest in mitosis, culminating in mitotic cell death (MCD) in HRS cells and not in solid tumor cells that we tested, perhaps because HRS cells notoriously harbor defective cell cycle regulation [22] and because of the pivotal role of anti-apoptotic proteins such as Bcl-2 in driving the survival of such cells [23,24]. Indeed we found that *N*-biphenylanilides caused a strong and early inactivation of Bcl-2 in HRS, instead this did not happen in solid tumors that we tested (unpublished data). Therefore we suggest that the inactivation of Bcl-2 was the critical event that triggered the MCD in HRS, instead different mechanistic pathways of cell death were induced by compounds in solid tumor cell lines. Because tumor angiogenesis greatly influences tumorigenesis either of solid tumors and hematological malignancies and that drugs belonging to the class of MTAs exert several antiangiogenic effects [25,26], we started the investigation of the antiangiogenic properties of *N*-biphenylanilides with PTA34, in order to provide a broader evaluation of biological effect of such compound. We found that, despite it did not inhibit the proliferation of either HMVEC and NHDF, thus suggesting a safety margin for this compound *in vivo*, it was very effective in inhibiting the capillary morphogenesis of human microvascular endothelial cells, perhaps because of its capability to inactivate Bcl-2, notoriously connected to proangiogenic functions [27–30].

Fundings

The study was supported by the fund of Ricerca Corrente 2016 (Ministry of Health) of IRCCS Istituto Tumori Giovanni Paolo II, Bari-Italy.

Conflicts of interest

None.

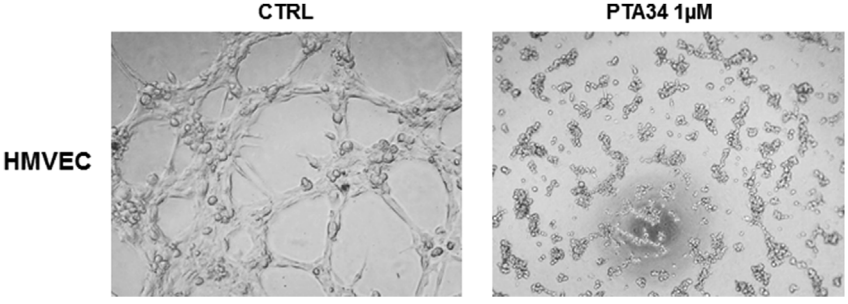

Fig. 8. Capillary morphogenesis after treatment with PTA34. Microvascular formation after 6 h from seeding on matrigel is reported in HMVEC untreated and 1 μM PTA34 treated specimens. Pictures shows how PTA34 completely disrupted the formation of microvascular formation.

Acknowledgements

The authors gratefully thank Prof. Rosaria De Filippi (University of Naples Federico II, Italy) who generously provided the Hodgkin lymphoma cell lines and Dr. Pinto Rosamaria and Dr. Petriella Daniela for the technical support in the preparation of DNA extracts from HRS cells.

Appendix A. Supplementary data

Supplementary data to this article can be found online at https://doi.org/10.1016/j.canlet.2018.12.013.

References

[1] K.S. Chan, C.G. Koh, H.Y. Li, Mitosis-targeted anti-cancer therapies: where they stand, Cell Death Dis. 3 (2012), https://doi.org/10.1038/cddis.2012.148 e411–e411.
[2] S. Haldar, A. Basu, C.M. Croce, Bcl2 is the guardian of microtubule integrity, Cancer Res. 57 (1997) 229–233 http://www.ncbi.nlm.nih.gov/pubmed/9000560.
[3] R.Z. Pellicani, A. Stefanachi, M. Niso, A. Carotti, F. Leonetti, O. Nicolotti, R. Perrone, F. Berardi, S. Cellamare, N.A. Colabufo, Potent galloyl-based selective modulators targeting multidrug resistance associated protein 1 and P-glycoprotein, J. Med. Chem. 55 (2012) 424–436, https://doi.org/10.1021/jm201305y.
[4] P. Tardia, A. Stefanachi, M. Niso, D.A. Stolfa, G.F. Mangiatordi, D. Alberga, O. Nicolotti, G. Lattanzi, A. Carotti, F. Leonetti, R. Perrone, F. Berardi, A. Azzariti, N.A. Colabufo, S. Cellamare, Trimethoxybenzanilide-based P-glycoprotein modulators: an interesting case of lipophilicity tuning by intramolecular hydrogen bonding, J. Med. Chem. 57 (2014) 6403–6418, https://doi.org/10.1021/jm500697c.
[5] M. Majellaro, A. Stefanachi, P. Tardia, C. Vicenti, A. Boccarelli, A. Pannunzio, F. Campanella, M. Coluccia, N. Denora, F. Leonetti, M. de Candia, C.D. Altomare, S. Cellamare, Investigating structural requirements for the antiproliferative activity of biphenyl nicotinamides, ChemMedChem 12 (2017) 1380–1389, https://doi.org/10.1002/cmdc.201700365.
[6] H.G. Drexler, C. Pommerenke, S. Eberth, S. Nagel, Hodgkin lymphoma cell lines: to separate the wheat from the chaff, Biol. Chem. 399 (2018) 511–523, https://doi.org/10.1515/hsz-2017-0321.
[7] L. Porcelli, E. Giovannetti, Y.G. Assaraf, G. Jansen, G.L. Scheffer, I. Kathman, A. Azzariti, A. Paradiso, G.J. Peters, The EGFR pathway regulates BCRP expression in NSCLC cells: role of erlotinib, Curr. Drug Targets 15 (2014) 1322–1330, https://doi.org/10.2174/1389450116666141205145620.
[8] S. Serratì, F. Margheri, M. Pucci, A.R. Cantelmo, R. Cammarota, J. Dotor, F. Borràs-Cuesta, G. Fibbi, A. Albini, M. Del Rosso, TGFβ1 antagonistic peptides inhibit TGFβ1-dependent angiogenesis, Biochem. Pharmacol. 77 (2009) 813–825, https://doi.org/10.1016/j.bcp.2008.10.036.
[9] B.T. Castle, S. McCubbin, L.S. Prahl, J.N. Bernens, D. Sept, D.J. Odde, Mechanisms of kinetic stabilization by the drugs paclitaxel and vinblastine, Mol. Biol. Cell 28 (2017) 1238–1257, https://doi.org/10.1091/mbc.E16-08-0567.
[10] I.E. Wertz, S. Kusam, C. Lam, T. Okamoto, W. Sandoval, D.J. Anderson, E. Helgason, J.A. Ernst, M. Eby, J. Liu, L.D. Belmont, J.S. Kaminker, K.M. O'Rourke, K. Pujara, P.B. Kohli, A.R. Johnson, M.L. Chiu, J.R. Lill, P.K. Jackson, W.J. Fairbrother, S. Seshagiri, M.J.C. Ludlam, K.G. Leong, E.C. Dueber, H. Maecker, D.C.S. Huang, V.M. Dixit, Sensitivity to antitubulin chemotherapeutics is regulated by MCL1 and FBW7, Nature 471 (2011) 110–114, https://doi.org/10.1038/nature09779.
[11] R. Chu, D.T. Terrano, T.C. Chambers, Cdk1/cyclin B plays a key role in mitotic arrest-induced apoptosis by phosphorylation of Mcl-1, promoting its degradation and freeing Bak from sequestration, Biochem. Pharmacol. 83 (2012) 199–206, https://doi.org/10.1016/j.bcp.2011.10.008.
[12] M. Marani, T. Tenev, D. Hancock, J. Downward, N.R. Lemoine, Identification of novel isoforms of the BH3 domain protein Bim which directly activate Bax to trigger apoptosis, Mol. Cell Biol. 22 (2002) 3577–3589, https://doi.org/10.1128/MCB.22.11.3577-3589.2002.
[13] E. Mukhtar, V.M. Adhami, H. Mukhtar, Targeting microtubules by natural agents for cancer therapy, Mol. Canc. Therapeut. 13 (2014) 275–284, https://doi.org/10.1158/1535-7163.MCT-13-0791.
[14] D.T. Terrano, M. Upreti, T.C. Chambers, Cyclin-dependent kinase 1-mediated bcl-xL/bcl-2 phosphorylation acts as a functional link coupling mitotic arrest and apoptosis, Mol. Cell Biol. 30 (2010) 640–656, https://doi.org/10.1128/MCB.00882-09.
[15] S. Mac Fhearraigh, M.M. Mc Gee, Cyclin B1 interacts with the BH3-only protein Bim and mediates its phosphorylation by Cdk1 during mitosis, Cell Cycle 10 (2011) 3886–3896, https://doi.org/10.4161/cc.10.22.18020.
[16] C.R. Han, D.Y. Jun, J.Y. Lee, Y.H. Kim, Prometaphase arrest-dependent phosphorylation of Bcl-2 and Bim reduces the association of Bcl-2 with Bak or Bim, provoking Bak activation and mitochondrial apoptosis in nocodazole-treated Jurkat T cells, Apoptosis 19 (2014) 224–240, https://doi.org/10.1007/s10495-013-0928-1.
[17] P. Nurse, Universal control mechanism regulating onset of M-phase, Nature 344 (1990) 503–508, https://doi.org/10.1038/344503a0.
[18] E.A. Nigg, Mitotic kinases as regulators of cell division and its checkpoints, Nat. Rev. Mol. Cell Biol. 2 (2001) 21–32, https://doi.org/10.1038/35048096.
[19] H.C. Vodermaier, APC/C and SCF: controlling each other and the cell cycle, Curr. Biol. 14 (2004) R787–R796, https://doi.org/10.1016/j.cub.2004.09.020.
[20] H. Puthalakath, D.C. Huang, L.A. O'Reilly, S.M. King, A. Strasser, The proapoptotic activity of the Bcl-2 family member Bim is regulated by interaction with the dynein motor complex, Mol. Cell. 3 (1999) 287–296 http://www.ncbi.nlm.nih.gov/pubmed/10198631.
[21] L. Du, C.S. Lyle, T.C. Chambers, Characterization of vinblastine-induced Bcl-xL and Bcl-2 phosphorylation: evidence for a novel protein kinase and a coordinated phosphorylation/dephosphorylation cycle associated with apoptosis induction, Oncogene 24 (2005) 107–117, https://doi.org/10.1038/sj.onc.1208189.
[22] A. Tzankov, S. Dirnhofer, Pathobiology of classical Hodgkin lymphoma, Pathobiology 73 (2006) 107–125, https://doi.org/10.1159/000095558.
[23] M. Bai, A. Papoudou-Bai, N. Horianopoulos, C. Grepi, N.J. Agnantis, P. Kanavaros, Expression of bcl2 family proteins and active caspase 3 in classical Hodgkin's lymphomas, Hum. Pathol. 38 (2007) 103–113, https://doi.org/10.1016/j.humpath.2006.06.017.
[24] A. Jayanthan, S.C. Howard, T. Trippett, T. Horton, J.A. Whitlock, L. Daisley, V. Lewis, A. Narendran, Targeting the Bcl-2 family of proteins in Hodgkin lymphoma: in vitro cytotoxicity, target modulation and drug combination studies of the Bcl-2 homology 3 mimetic ABT-737, Leuk. Lymphoma 50 (2009) 1174–1182, https://doi.org/10.1080/10428190902943069.
[25] E. Pasquier, S. Honoré, D. Braguer, Microtubule-targeting agents in angiogenesis: where do we stand? Drug Resist. Updates 9 (2006) 74–86, https://doi.org/10.1016/j.drup.2006.04.003.
[26] M.-D. Canela, S. Noppen, O. Bueno, A.E. Prota, K. Bargsten, G. Sáez-Calvo, M.-L. Jimeno, M. Benkheil, D. Ribatti, S. Velázquez, M.-J. Camarasa, J.F. Díaz, M.O. Steinmetz, E.-M. Priego, M.-J. Pérez-Pérez, S. Liekens, Antivascular and antitumor properties of the tubulin-binding chalcone TUB091, Oncotarget 8 (2017) 14325–14342, https://doi.org/10.18632/oncotarget.9527.
[27] A. Biroccio, A. Candiloro, M. Mottolese, O. Sapora, A. Albini, G. Zupi, D. Del Bufalo, Bcl-2 overexpression and hypoxia synergistically act to modulate vascular endothelial growth factor expression and in vivo angiogenesis in a breast carcinoma line, FASEB J. 14 (2000) 652–660 http://www.ncbi.nlm.nih.gov/pubmed/10744622.
[28] E. Karl, K. Warner, B. Zeitlin, T. Kaneko, L. Wurtzel, T. Jin, J. Chang, S. Wang, C.Y. Wang, R.M. Strieter, G. Nunez, P.J. Polverini, J.E. Nör, Bcl-2 acts in a proangiogenic signaling pathway through nuclear factor-κB and CXC chemokines, Cancer Res. 65 (2005) 5063–5069, https://doi.org/10.1158/0008-5472.CAN-05-0140.
[29] M. Diensthuber, M. Potinius, T. Rodt, A.C. Stan, H.J. Welkoborsky, M. Samii, J. Schreyögg, T. Lenarz, T. Stöver, Expression of bcl-2 is associated with microvessel density in olfactory neuroblastoma, J. Neuro Oncol. 89 (2008) 131–139, https://doi.org/10.1007/s11060-008-9602-9.
[30] A. Fernandez, T. Udagawa, C. Schwesinger, W. Beecken, E. Achilles-Gerte, T. McDonnell, R. D'Amato, Angiogenic potential of prostate carcinoma cells overexpressing bcl-2, J. Natl. Cancer Inst. 93 (2001) 208–213 http://www.ncbi.nlm.nih.gov/pubmed/11158189.